

## **MASTER OF PHILOSOPHY Modelling of Materials 2005**

### Examiners' Solutions to Paper 1

#### SECTION A

##### 1(a)

The distinction between a model and a theory is not straightforward since practitioners often use the two terms interchangeably. It can even become a matter of philosophical debate. Therefore any well-reasoned answer is acceptable. One approach based on reductionism would go as follows:

A theory in materials science is a set of scientific principles or propositions based on proven laws of physics and chemistry. It can be mathematically rigorous, is usually expressed in terms algebraic, differential or integral equations and attempts to predict observable quantities. It can exist at various levels of complexity and may or may not have an analytical solution. Examples include dislocation theory, nucleation theory, free electron theory, kinetic theory etc.

A model is a reduced or idealised theory that removes complicating factors and captures only essential features. It focuses on observables using simplified state equations. It may involve parametric fitting to experimental data and may or may not have an analytical solution. Examples include the pair potential model for solids, the Ising model for phase transitions, cellular models for microstructural evolution and neural network models for interpolating complex materials data.

Synergism is a cooperative action such that the total effect is greater than the sum of the effects taken independently. In the case of modelling, theory and experiment the idea is that their combined application to a problem in materials science will have a greater effect than if either method were used alone. The coupling between theory, modelling and experiment also serves to validate the model and confirm the experimental observations.

##### 1(b)

The Embedded Atom Method (EAM) is an empirical implementation of Effective Medium Theory for the binding energy of a metal. This energy is written as two terms, one for the attractive energy of embedding each atom in the electron density provided by neighbouring atoms, and another

describing the electrostatic repulsive overlap interaction of neutral atoms. Thus the binding energy is given by:

$$U = \sum_i F(\rho_i) + \frac{1}{2} \sum_{i \neq j} \phi(r_{ij})$$

where  $\rho_i = \sum_{i \neq j} \rho^A(r_{ij})$  which is the charge at the  $i$ th nucleus due to the spherically symmetric *atomic* charge densities  $\rho^A(r_{ij})$  of neighbouring atoms.  $F(\rho_i)$  is the embedding function and  $\phi(r_{ij})$  is a pair potential describing the overlap interaction. Both the embedding function and pair potential are parametrically fitted to match various bulk and defect properties of the metal concerned.

The form of  $F(\rho_i)$  is chosen to reflect the fact that the energy of an atom is a *non-linear* function of the coordination number. This function is concave negative and in a related model by Finnis and Sinclair takes a (negative) square root form.

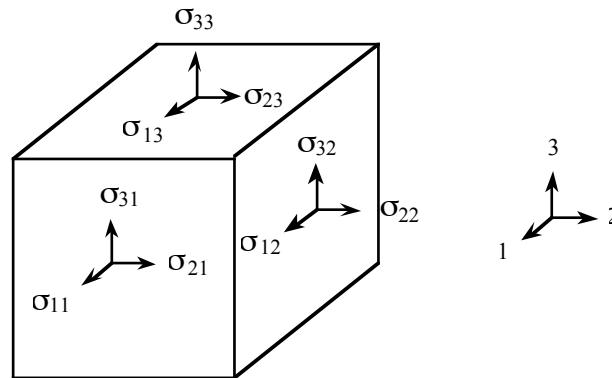
Previous methods for simulating metals have used pair potentials to describe *all* the binding energy. These methods erroneously predict the Cauchy relation for the elastic constants of a cubic metal ( $c_{12} = c_{44}$ ) and do not give a bond strength which increases as the coordination number decreases. EAM successfully overcomes both of these previous deficiencies.

1(c)

Answer to include descriptions of at least three of the following methods: Cooling curves; Metallography; X-ray diffraction; Dilatometry; Electrical conductivity.

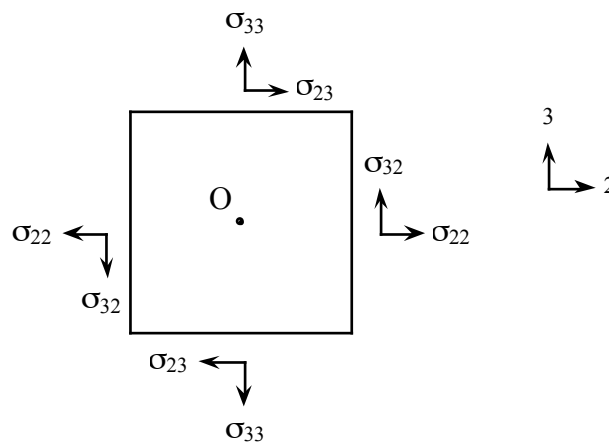
1(d)

For a general stress state imposed upon a unit cube within a material, we have:



using the convention that  $\sigma_{ij}$  denotes a stress in the 'i' direction on the 'j' face. Stresses of the form  $\sigma_{ii}$  are tensile stresses and stresses of the form  $\sigma_{ij}$  ( $i \neq j$ ) are shear stresses.

If we examine the forces acting on the 2-3 section of the unit cube (i.e., looking towards the cube anti-parallel to the '1' axis), we have:



If we take moments about 'O':

$$\text{Sum of clockwise moments} = \frac{\sigma_{23}}{2} + \frac{\sigma_{23}}{2} = \sigma_{23}$$

$$\text{Sum of anticlockwise moments} = \frac{\sigma_{32}}{2} + \frac{\sigma_{32}}{2} = \sigma_{32}$$

So the condition that the cube is in static equilibrium (i.e., for this section, it does not rotate about the '1' axis) requires  $\sigma_{23} = \sigma_{32}$ .

Similarly, looking at the 1-2 and 3-1 sections of the cube, we find  $\sigma_{12} = \sigma_{21}$  and  $\sigma_{31} = \sigma_{13}$  respectively. Hence we have shown  $\sigma_{ij} = \sigma_{ji}$  for  $i \neq j$ .

For the stress state

$$\sigma = \begin{pmatrix} \sigma_{11} & \sigma_{12} & 0 \\ \sigma_{12} & \sigma_{22} & 0 \\ 0 & 0 & \sigma_{33} \end{pmatrix}$$

we simply need to find the eigenvalues of the matrix to specify the principal stresses.

Clearly, by inspection, one of the principal stresses is  $\sigma_{33}$ .

The other two principal stresses can be found by solving the 2x2 determinant

$$\begin{vmatrix} \sigma_{11} - \lambda & \sigma_{12} \\ \sigma_{12} & \sigma_{22} - \lambda \end{vmatrix} = 0$$

Solving the determinant, we have:

$$(\sigma_{11} - \lambda)(\sigma_{22} - \lambda) - \sigma_{12}^2 = 0$$

whence the two other principal stresses are

$$\lambda = \frac{(\sigma_{11} + \sigma_{22})}{2} \pm \sqrt{\left(\frac{\sigma_{11} - \sigma_{22}}{2}\right)^2 + \sigma_{12}^2}$$

Hence the three principal stresses are

$$\sigma_{33} \text{ and } \frac{(\sigma_{11} + \sigma_{22})}{2} \pm \sqrt{\left(\frac{\sigma_{11} - \sigma_{22}}{2}\right)^2 + \sigma_{12}^2}$$

1(e)

```
subroutine tspose (t)
  implicit none
  real temp
  real t(10,10)
  integer i, j
  do 10, i = 1, 9
    do 10, j = i+1, 10
      temp = t(i,j)
      t(i,j) = t(j,i)
      t(j,i) = temp
10 continue
  return
end
```

1(f)

The distinguishing feature is that a crystalline material exhibits long-range order whereas an amorphous material does not. Crystalline materials include the vast majority of metals in their equilibrium states. Amorphous materials include metallic glass, silica glass, glassy polymers such as PMMA (acrylic).

An amorphous solid can be made by cooling a liquid at a rate that is fast enough to suppress crystallisation. Glassy metallic alloys generally have to be cooled at around  $10^6$  K/s, although there are complex alloys that become glassy at much lower cooling rates. Window glass remains glassy even when cooled slowly, because silica molecules are strongly bonded into a huge three-dimensional network.

1(g)

Fick's law states: 
$$J_A = -D_A \frac{\partial C_A}{\partial x}$$

However, diffusion is driven by a free energy gradient. The free energy of  $A$  is  $C_A \mu_A$  so we should write:

$$J_A = -C_A M_A \frac{\partial \mu_A}{\partial x} \text{ so that } D_A = C_A M_A \frac{\partial \mu_A}{\partial C_A}$$

It is necessary to consider the free energy gradient when dealing with non-ideal solutions, e.g. phase separation that occurs in a miscibility gap. Uphill diffusion occurs (i.e from low  $A$  concentration to high  $A$  concentration) and the driving force cannot simply be the concentration gradient.

1(h)

An artificial neural network is a parameterised non-linear mapping between inputs and outputs. The architecture consists of a series of nodes with multiple connections to other nodes. Each connection has a weight  $w_j$  associated with it. Each node sums the weighted combination of its inputs  $y = \sum_i w_i x_i$ . This value passes through a non-linear transform function acting as a "hidden layer" e.g.,

$$z = \tanh(y) \text{ or } z = 1/(1 + e^{-\lambda y})$$

The output  $z$  is passed on to every node in the next layer. The network can have several hidden layers and transform functions. The key is adapting the weights  $w_i$  to yield known target output and then using these  $w_i$  on new input (this is called training the network).

The advantages of ANN: can model non-linear problems with many parameters; can model complex materials phenomena for which physical models not exist; is highly adaptable (amount and type of input data can be altered).

The disadvantage of ANN: can be used blindly without any physical insight or fundamental understanding of the properties or processes being modelled.

1(i)

*Advantages*

Analytical	Numerical
Simple to compute (e.g. spreadsheet), and sufficient for some simple problems	Ability to handle complexity (in geometry, multiple materials in the problem, spatially or time-varying boundary conditions, temperature-dependent properties)
Useful to guide setting up an efficient numerical solution, and checking numerical solution works	
Map results over wide domain of input parameters	
Well-suited to thorough sensitivity analysis	

*Disadvantages*

Analytical	Numerical
Limited to idealised situations (constant properties, simple boundary conditions, approximated geometries such as semi-infinite etc)	Greater computational complexity, with greater burden of input data required, but too easy to use without sufficient validation and checking
	Each computation for single set of conditions – cumbersome to span a wide parameter space, and too rarely used for sensitivity analysis

1(j)

The united atom approximation involves replacing each CH<sub>2</sub> or CH<sub>3</sub> unit in a hydrocarbon polymer molecule with a single united atom with an effective mass of 14 or 15 g mol<sup>-1</sup> with force field parameters that are adjusted so as to model the steric interactions between the missing hydrogen atoms. The advantages of this are two-fold: (i) it reduces the number of atoms in the MD simulation, and (ii) it eliminates the high-

frequency C–H bond stretching and bending modes from the simulation. Although (i) will accelerate the simulation by reducing the total number of atoms in the system, by far the most important factor is (ii), which enables a much shorter time step to be used in the dynamics simulation without numerical instability. Generally, it is the integration of the short time period (around 11 fs) C–H bond stretching modes that limit the maximum rate at which the forces in the simulation can be integrated – the typical time step used is 1 fs. However, elimination of the C–H stretching motions means time steps up to 5 fs can be used without instability, giving a speed up of around 500%, which is more significant than the speed up due to the reduction of the number of atoms.

Other methods to accelerate dynamical simulations of hydrocarbons include the use of bond constraints (using SHAKE or RATTLE algorithms), which again freeze out the C–H bond stretching modes, but without eliminating the detailed steric interactions between the hydrogen atoms. This is generally a superior approach to using the united atom model, as the presence or absence of hydrogens will strongly affect the chain packing in the crystalline solid form (e.g. united atom model might predict hexagonal structure for crystalline polyethylene, whereas the actual structure is orthorhombic). Freezing out the C–H bond bending motions can also be achieved using SHAKE or RATTLE, although the time saving is hardly worth the extra computational expense of enforcing the constraints. However, full rigid body dynamics is not appropriate as there could be no conformational relaxation of the polymer, which is important in both solid and melt states. Lastly, multiple time step algorithms, where the different degrees of freedom in the molecule are integrated at different rates, could also be used effectively, but are more computationally expensive than using bond constraints and require careful choice of the relative time step parameters to produce a stable simulation. In summary, united atom models can only really be successful for the simulation of hydrocarbon melts or low density glassy phases, whereas bond constraints would be a much more suitable method for simulating high density solids and crystalline phases.

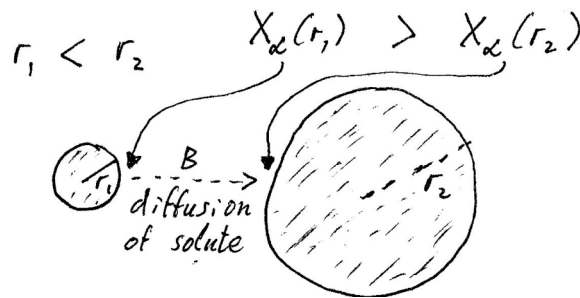


## SECTION B

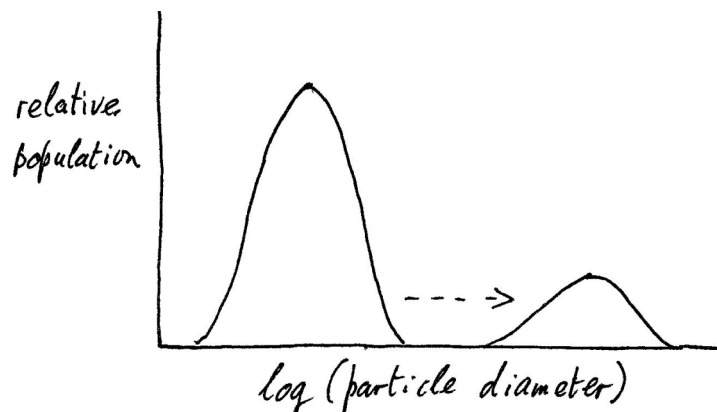
2.

Ostwald ripening is the coarsening of a precipitate dispersion (i.e. evolution towards fewer bigger particles, at inevitably greater separation), at essentially constant volume fraction of particles. The greater separation of the particles permits bowing of dislocations between them; the bowing stress is inversely proportional to the separation, and so ripening leads to softening of precipitation-hardened alloys. [15%]

The driving force is reduction of the interfacial area between particles and matrix. As a result of the diffusional fluxes of B atoms in the matrix, the smaller particles shrink while the bigger particles grow. The shrinkage of the smaller particles is an essential part of the coarsening process as their eventual disappearance reduces the population of particles — necessary if the average particle size is to increase while keeping their total volume fraction constant.



The particle size distribution is typically log-normal, and evolves to increased average particle diameter with constant width of distribution (and reduced height, as total volume fraction is constant).



[25%]

The derivation is bookwork, and proceeds (in outline) as follows. The key assumption (consistent with the above sketch) is that the particle size distribution remains self-similar throughout. The ripening involves diffusional fluxes of B atoms from smaller to bigger particles. The enhancements of equilibrium solute contents in the matrix (compared to that in contact with a planar interface) due to finite particle size are

inversely proportional to particle radius  $r$ . Thus the composition differences driving these fluxes are inversely proportional to the average radius  $\bar{r}$ . The diffusion distances are proportional to  $\bar{r}$ , and thus the composition gradients are proportional to  $1/\bar{r}^2$ . The rate of change of  $\bar{r}$  must scale with the diffusional fluxes, and therefore with  $1/\bar{r}^2$ . Integrating

$$\frac{d\bar{r}}{dt} \propto \frac{1}{\bar{r}^2}$$

gives

$$\bar{r}^3(t) - \bar{r}^3(0) \propto t .$$

[30%]

The key parameters are those which control the diffusional fluxes. Obviously a lower solute diffusivity would be desirable to inhibit coarsening. The composition differences (i.e.,  $X_\alpha(r_1) - X_\alpha(r_2)$ ) must also be reduced. This can be achieved by reducing the interfacial energy  $\gamma$  and the equilibrium solute solubility  $X_\alpha(\infty)$ .

[15%]

The most important assumption is that there is a single well-defined particle size distribution which remains self-similar throughout the process. The evolution towards this distribution from an arbitrary starting distribution is clearly not modelled in this simple approach. Nor can the approach deal with bimodal or more complex size distributions. A bimodal size distribution is quite likely, for example, when precipitation occurs in a polycrystalline matrix. In that case larger precipitates are expected on the grain boundaries (especially at junctions), and finer precipitates in grain interiors. The spatial distribution of these precipitates is also not random, as there are likely to be zones around the large particles in which the population of small particles is depleted. A full model could also take account of spatially varying temperature or overall matrix solute content, such as are likely to arise in real alloys under real processing.

[15%]

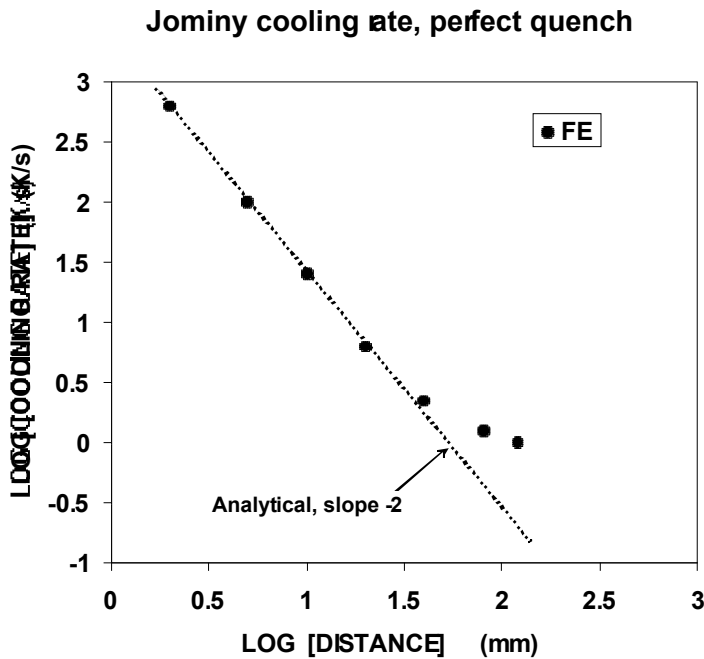
3.

(a) Boundary conditions: Sides of bar (and remote end in FE analysis): thermally insulated. Quenched end: perfect heat transfer ( $T = \text{ambient}$ , for all  $t > 0$ ). Initial temperature uniform along the bar. Number and type of elements: 20 linear elements (although 2 to 5 quadratic elements also fine)

[20%]

(b) Log-log plot of FE results:

x (mm)	dT/dt (K/s)	log (x)	log (dT/dt)
2	631	0.301	2.80
5	100	0.700	2.00
10	25.1	1.00	1.40
20	6.31	1.301	0.80
40	2.24	1.602	0.35
80	1.26	1.903	0.10
120	1	2.079	0.00



From the analytical solution, expected slope on log-log plot is -2. FE data has correct slope towards the quenched end, but deviates to faster cooling rates than expected from an extrapolation of this slope, towards the remote end of the bar. This is because the real bar (and the FE solution) have a finite length, whereas the analytical solution is for a semi-infinite solid. Near the quenched end the discrepancy is negligible, but at the remote end the FE cools faster than the analytical, since heat continues to enter the bar at  $x=120\text{mm}$  in the analytical solution, which is not the case in practice (retarding the cooling rate). [50%]

(c) Hence the line of slope -2 should be fitted to the FE data at the quenched end. Solving for the constant C, e.g. by plugging in the data for

$x = 5\text{mm}$ , as there is no scatter in the initial linear part of the FE data:  $C = 2.5 \times 10^3 \text{ mm}^2\text{s/K}$  (note units must be consistent with data). [30%]

4.

Regression analysis is most frequently used in circumstances where the physical relationship between the input and output variables is not known. With linear regression, one begins at the outset with the assumption that the relationship will be linear or pseudo-linear (i.e., contain additive terms). [20%]

By contrast, a neural network makes no such assumption but is able to capture complex, non-linear relationships and interdependencies between variables. This is because any number of hyperbolic tangents (or other transfer functions) can be combined to capture the complex patterns in the data. [20%]

In a linear regression method, once established, a regression equation and its associated straight line applies across the entire domain of data. There are many circumstances in which the dependence of the output on a particular input may be quite different in different regions of the input space. For example, the strength of steel increases with carbon concentration, but beyond the point where graphite precipitates, it can lead to a major reduction in tensile strength. [20%]

A neural network is sufficiently flexible to capture such changes in behaviour and to fit the mathematical function appropriately. In linear regression, dependencies between variables have to be expressed at the outset, for example by writing  $y = w_1x_1 + w_2x_2 + w_{12}x_1x_2$ , where the  $w_i$  are coefficients derived by fitting and  $x_i$  the input variables. The third term is clearly an arbitrarily constructed dependency which may or may not be justified. [20%]

Neural networks on the other hand capture the dependencies from the data since a function does not need to be defined at the beginning of the analysis – its form is an outcome of the analysis. [20%]

5.

Denoting time derivatives by the usual convention of dots above the characters, then the Lagrangian for a standard Hamiltonian system can be written as

$$L = \frac{1}{2} \sum_i^N m_i \dot{x}_i^2 - V(x_i)$$

where  $\dot{x}_i$  are the particle velocities,  $x_i$  the particle positions and  $m_i$  the masses.  $V(x_i)$  is a scalar potential which is a function of the particle positions only. Substituting  $L$  into the Euler-Lagrange equations, one obtains:

$$\frac{\partial L}{\partial \dot{x}_i} = m_i \dot{x}_i \quad \frac{\partial L}{\partial x_i} = -\frac{\partial V}{\partial x_i}$$

$$\therefore \frac{d}{dt} \frac{\partial L}{\partial \dot{x}_i} - \frac{\partial L}{\partial x_i} = \frac{d}{dt} (m_i \dot{x}_i) + \frac{\partial V}{\partial x_i} = 0$$

$$\therefore \frac{d}{dt} (m_i \dot{x}_i) = -\frac{\partial V}{\partial x_i}$$

which is the usual form of Newton's second law, with rate of change of momentum on LHS, and force on the RHS.

[30%]

If  $L$  is augmented by an extra coordinate  $\zeta$ , which evolves in time so as to minimise the difference between the instantaneous kinetic and statistical temperatures,  $T_K$  and  $T_S$  respectively, then  $T_S$  becomes a parameter of the simulation and  $T_K$  fluctuates. This is the basis of the Nosé-Hoover thermostatting method for producing molecular dynamics trajectories in the canonical ensemble.

The kinetic temperature is defined by averaging over all kinetic degrees of freedom, i.e.:

$\frac{1}{2} \sum_i^N m_i \dot{x}_i^2 = \frac{3Nk_B T_K}{2}$  by equipartition, which will fluctuate in equilibrium by definition.

The statistical temperature is defined from the Boltzmann distribution of microstate occupancies once equilibrium has been obtained, i.e.:

$p_i = \frac{\exp(-E_i/k_B T_S)}{\sum_i \exp(-E_i/k_B T_S)}$ , which should be constant at equilibrium by definition.

The other terms in the Nosé-Hoover equations of motion are the particle velocities  $\dot{r}_i$ , momenta  $p_i$ , rates of change of momenta  $\dot{p}_i$  and forces  $E_i$ . The parameter  $\tau_T$  is known as the thermostat relaxation time, and has units of time. It controls the rate at which energy can flow back and forth from the thermostat reservoir to the system. Its value must be chosen carefully to ensure that a stable equilibrium temperature is evolved, and that the system remains ergodic. This can be checked by plotting the kinetic temperature as a function of time. If the system is overdamped, then  $T_K$  will converge only slowly on  $T_S$  resulting in an inefficient thermostat. If the system is underdamped, then  $T_K$  will oscillate about  $T_S$ , resulting in a loss of ergodicity. The typical range of  $\tau_T$  for critical damping is between 0.5 to 2 ps, but this depends very much on the system being simulated. It is also a good idea to check the residuals of  $T_K$  about  $T_S$ . These should be Gaussian, and multimodal or highly skew distributions are a warning sign that the system is not ergodic. This is known to happen for very simple systems such as the harmonic oscillator, and can be ameliorated to a certain extent by chaining together thermostats with a spectrum of relaxation times.

[50%]

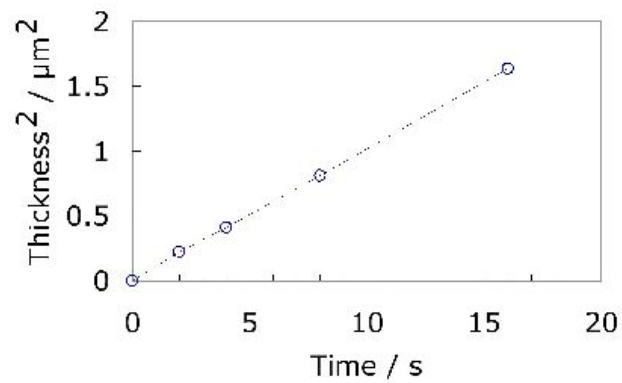
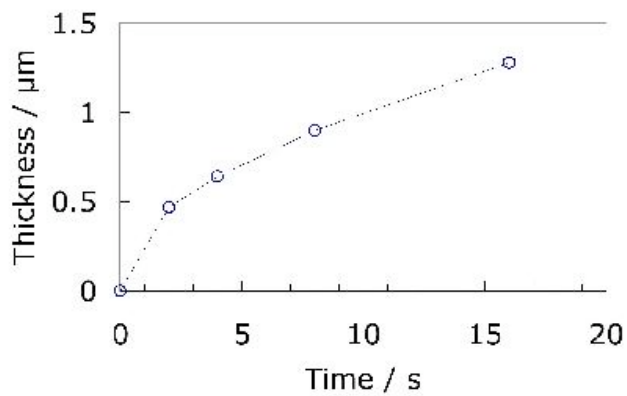
Hybrid MC/MD thermostatting schemes, such as the Andersen method which involves stochastic collisions between particles and a heat reservoir, produce a canonical NVT distribution and are also used instead of deterministic schemes like Nosé-Hoover. They have the advantages that they are usually quicker and more efficient at equilibrating than deterministic schemes, but the disadvantages that they can be difficult to combine with constraint dynamics (SHAKE) or dynamic perturbations like shear forces. Also, most implementations of Andersen's method only cater for isotropically varying periodic cells, unlike the extended Lagrangian approaches that are easily generalized to anisotropic cell fluctuations.

[20%]

SECTION C

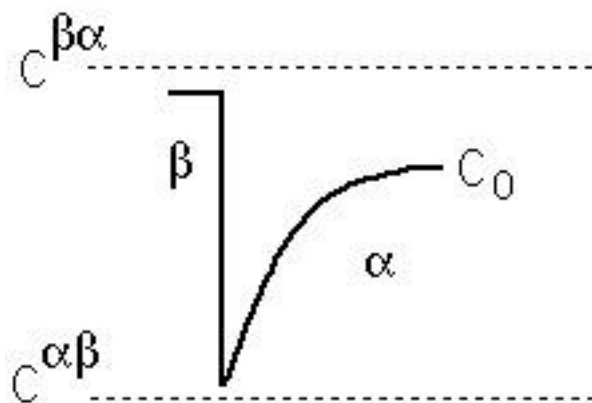
6.

The figures below show that the relationship between thickness and time is parabolic, indicating that growth is diffusion-controlled.



[20%]

The composition profile at the interface is illustrated below:



[20%]

The diffusion flux of solute towards the interface must equal the rate at which solute is incorporated in the precipitate so that:

$$(C^{\beta\alpha} - C^{\alpha\beta}) \frac{\partial x^*}{\partial t} = D \left. \frac{\partial C}{\partial x} \right|_{x=x^*} \equiv D \frac{C_0 - C^{\alpha\beta}}{\Delta x}$$

where  $\Delta x$  is the diffusion distance in the matrix ahead of the interface assuming a constant gradient. A second equation can be derived by considering the overall conservation of mass:

$$(C^{\beta\alpha} - C_0) x^* = \frac{1}{2} (C_0 - C^{\alpha\beta}) \Delta x$$

On combining these expressions to eliminate  $\Delta x$  we get:

$$\frac{\partial x^*}{\partial t} = \frac{D (C_0 - C^{\alpha\beta})^2}{2 x^* (C^{\beta\alpha} - C^{\alpha\beta}) (C^{\beta\alpha} - C_0)}$$

This can be integrated to show that  $x^{*2} \propto t$ . [40%]

The approximations: assumes a constant concentration gradient, that the far-field composition  $C_0$  remains constant, that diffusion is one-dimensional, that the diffusion coefficient is composition independent.

[20%]

7.

When the pure phases are  $\alpha$  and  $\gamma$  and in equilibrium their Gibbs free energies are equal:  $G^\alpha = G^\gamma$ . [10%]

Consider  $\alpha$  consisting of two components  $A$  and  $B$ . The free energy of  $\alpha$  is a function of the mole fractions  $(1 - x)$  and  $x$  of  $A$  and  $B$  respectively:

$$G^\alpha = (1 - x)\mu_A + x\mu_B$$

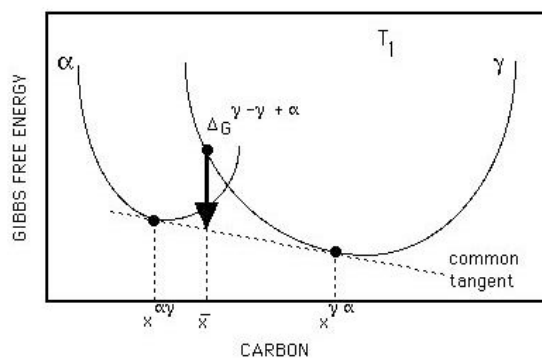
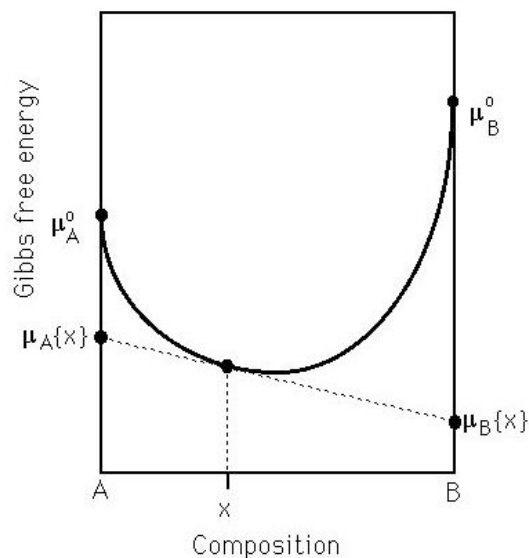
where  $\mu_A$  represents the mean free energy of a mole of  $A$  atoms in  $\alpha$ . The term  $\mu$  is called the chemical potential of  $A$ . Thus the free energy of a phase is simply the weighted mean of the free energies (chemical potentials) of its component atoms.



Consider now the coexistence of two phases  $\alpha$  and  $\gamma$  in the binary alloy. They will only be in equilibrium with each other if the  $A$  atoms in  $\alpha$  have the same free energy as the  $A$  atoms in  $\gamma$ , and if the same is true for the  $B$  atoms:

$$\begin{aligned}\mu_A^\alpha &= \mu_A^\gamma \\ \mu_B^\alpha &= \mu_B^\gamma\end{aligned}$$

The condition the chemical potential of each species of atom must be the same in all phases at equilibrium is general and justifies the common tangent construction as illustrated in the figure. Notice that the common tangent gives identical intercepts for both  $\alpha$  and  $\gamma$  at  $x = 0$  and  $1 - x = 0$ .



[50%]

When the solution consists of a random dispersion of atoms, the entropy of mixing is as given,

$$\Delta S_{M1} = -kN \left[ \left( \frac{N-n}{N} \right) \ln \left\{ \frac{N-n}{N} \right\} + \frac{n}{N} \ln \left\{ \frac{n}{N} \right\} \right]$$

When a single cluster of  $t$   $B$ -atoms forms, the number of  $B$  entities is reduced to  $n - t + 1$ , the  $+1$  representing the single cluster. The entropy of mixing is then:

$$\Delta S_{M2} = -k(N-t+1) \left[ \left( \frac{N-n}{N-t+1} \right) \ln \left\{ \frac{N-n}{N-t+1} \right\} + \frac{n-t+1}{N-t+1} \ln \left\{ \frac{n-t+1}{N-t+1} \right\} \right]$$

The change in entropy is therefore given by:

$$\begin{aligned} \Delta S &= \Delta S_{M2} - \Delta S_{M1} \\ &= -k \left( (N-n) \ln \left( \frac{N-n}{N-t+1} \right) - (N-n) \ln \left( \frac{N-n}{N} \right) - n \ln \left( \frac{n}{N} \right) + (n-t+1) \ln \left( \frac{n-t+1}{N-t+1} \right) \right) \end{aligned}$$

$$\cong k(t-1) \ln \{x\}$$

$$\text{since } \frac{n-t+1}{N-t+1} \cong \frac{n}{N} \quad \text{and} \quad \frac{N-n}{N-t+1} \cong \frac{N-n}{N}$$

[40%]